Design and Kinematic Analysis of a Single-Degree-of-Freedom Rigidly Foldable Winding Origami Pattern

Sibo Chai, Jiayao Ma, Kaili Xi, and Yan Chen

Abstract The winding origami structure allows the panels to be wrapping folded to achieve a very large deployable ratio. However, the existing winding origami patterns are non-rigidly foldable or multi-degree-of-freedom rigidly foldable. In this paper, a new single-degree-of-freedom rigidly foldable winding origami pattern is designed based on a non-rigidly foldable winding origami pattern. The new pattern is obtained by removing the creases in the area of concentrated panel deformation under non-rigidly folding and then converting the generated virtual creases into actual creases. The panel deformation and folding energy are reduced through the crease transformation. The kinematic analysis by the truss transformation method proves its rigidly foldable characteristics with one degree of freedom. Therefore, this pattern design has an application prospect in aerospace engineering and emergency equipment. In addition, it provides an idea for the transition from non-rigid structures to rigid ones which also has universal significance.

Keywords Winding origami · Rigid foldability · Crease transformation · Kinematic analysis

1 Introduction

Origami is an ancient art of folding the complete sheets of paper to form complex 2D or 3D structures without cutting and bonding. Origami structures have excellent deployable characteristics, diverse design parameters and simple manufacture, which have been widely researched in the field of aerospace deployable structures [1, 2] and many others [3–5].

S. Chai · J. Ma · K. Xi · Y. Chen (✉)
Key Laboratory of Mechanism and Equipment Design of Ministry of Education, Tianjin University, Tianjin 300350, China
e-mail: yan_chen@tju.edu.cn

School of Mechanical Engineering, Tianjin University, Tianjin 300350, China

X. Liu (ed.), *Advances in Mechanism, Machine Science and Engineering in China*,
Lecture Notes in Mechanical Engineering,
https://doi.org/10.1007/978-981-19-9398-5_88

Depending on the folding motion, origami can be divided into rigidly foldable origami and non-rigidly foldable origami. In the folding process of rigidly foldable origami, the panels never stretch or bend, but just rotate around the crease [6]. The folding of rigidly foldable origami is essentially a mechanism movement, and the panel and creases can be equivalent to the rigid connecting rod and revolute joint respectively [7, 8]. Many methods have been proposed to judge the stiffness of rigidly foldable origami structures, such as numerical algorithm [9], matrix method [10], kinematic method [7, 11], etc. For non-rigidly foldable origami, crease rotation and panel deformation occur simultaneously. Although the theoretical modeling is difficult, it can achieve richer mechanical properties, such as high bearing capacity and high energy absorption [12], bistable [13] and variable stiffness [14].

Winding origami is a type of origami structure that can realize wrapping folding with a large deployable ratio, which has been widely used in many engineering fields, such as solar arrays [15] and frequency-reconfigurable antennas [16]. Guest and Pellegrino [17] first proposed an origami wrapping pattern around the center whose panels in the flat and tightly winding states are not stretched but not necessarily in transition between the two states. The Flasher origami pattern is also a typical non-rigidly foldable winding origami with rotational symmetry, which is flat in the unfolded state, cylindrical in the folded state, and unfolds in a spiral mode [18–20]. The Flasher origami structure allows the winding surface to be folded multiple times, ensuring that the diameter and height of the winding column are approximately constant. In addition, Xu et al. [15] proposed a winding origami pattern with bistable characteristics. Liu et al. [21] analyzed its kinematic relationship which reveals its folding process with a single degree of freedom in the rigid stage and studied the mechanical response and local deformation of the panels in the non-rigid stage.

Without panel deformation, rigidly foldable origami is suitable for the design of deployable structures. Many studies add creases [22] or cut along creases [23] of the non-rigidly winding patterns to achieve rigidity, but both of them have multiple degrees of freedom. In this work, to realize the rigid foldability of the winding structure with one degree of freedom, a new pattern is designed through the exploration of the deformation of a non-rigidly foldable winding origami [21] (shown in Fig. 1). The folding characteristic of the new pattern is compared with the original one in Sect 2. The kinematics analysis is carried out through the truss transformation and proves its rigidly foldable characteristics with one degree of freedom in Sect 3.

2 Geometric Design of the New Pattern

2.1 The Non-rigidly Foldable Pattern and Experimental Setup

The crease pattern of the non-rigidly foldable winding origami is shown in Fig. 1a [21], where the solid line represents the mountain line, the dotted line represents

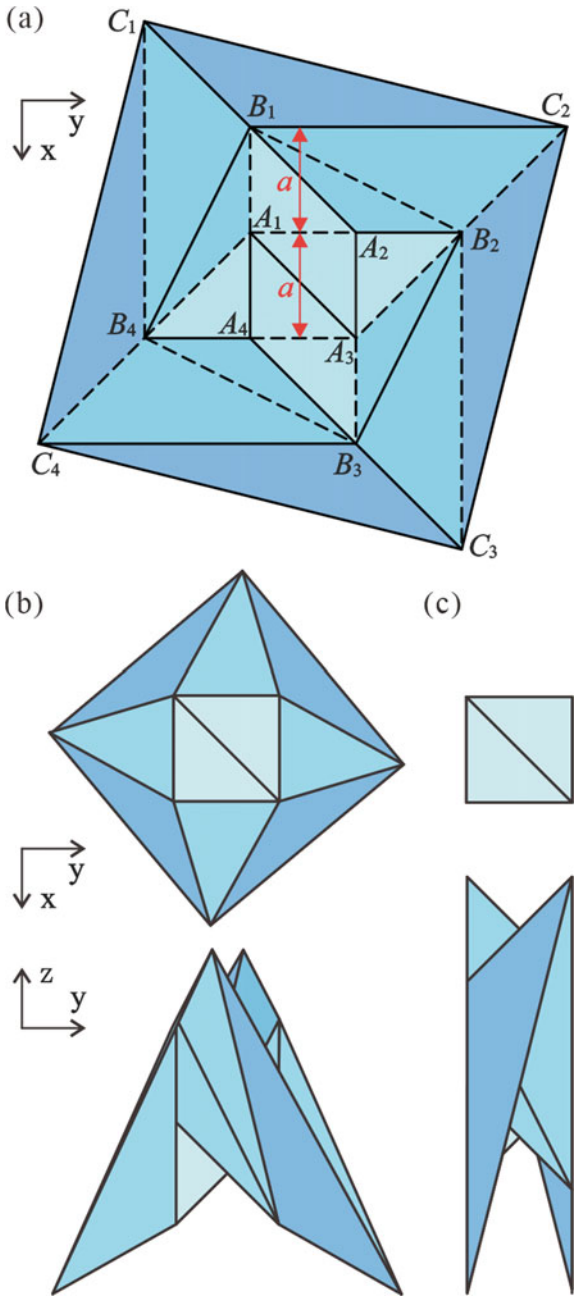

Fig. 1 The geometry design and folding process of a non-rigidly foldable winding origami: **a** crease pattern (flat state point), **b** self-locking state point, **c** tightly winding state point

the valley line, and the color from light to dark represents the layer from inside to outside. The structure is rotationally symmetric, and the geometric dimension can be entirely determined by parameters a. Figure 1a–c shows the folding process of the structure in the simulation software (Solidworks), which can be divided into two stages, the rigidly foldable stage from Fig. 1a to b and the non-rigidly foldable stage from Fig. 1b to c. The state point in Fig. 1b is the critical position of the structure from the rigidly foldable stage to the non-rigidly foldable stage, namely the self-locking point. Figure 1b and c are the two stable state points of the origami structure whose panels are not deformed (no penetration in simulation).

Physical specimens are made to investigate the deformation mode of the non-rigidly foldable winding structure. For all specimens, the dimension parameter is set to $a = 30$ mm. PET panels with thickness $t = 0.30$ mm are used. The creases are cut off 1.9 mm at 0.6 mm intervals with a width of 0.3 mm. Circular holes with a radius $r = 1$ mm are cut at the intersection of creases to avoid stress concentration. The material properties of PET are as follows: density $\rho = 1.37$ g/cm3, Young's modulus $E = 3010$ MPa, yield stress $\sigma_y = 64.5$ MPa. The specimen of the non-rigidly foldable winding origami is shown in Fig. 2 and its flat state point is shown in Fig. 3b.

At the same time, a 304 stainless steel frame with a thickness of 2 mm is made. The frame moves with a single degree of freedom when only the horizontal displacement is allowed on both loading ends. The motion trail of the inner boundary of the frame

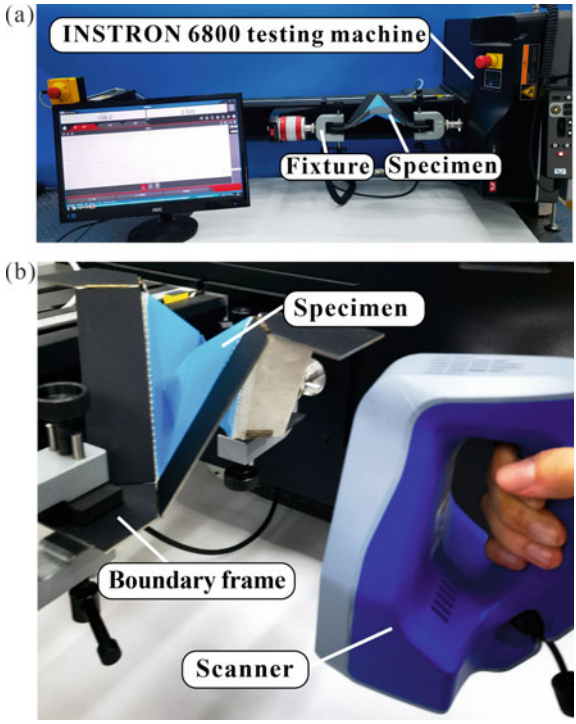

Fig. 2 Folding test and 3D scanning experimental setup

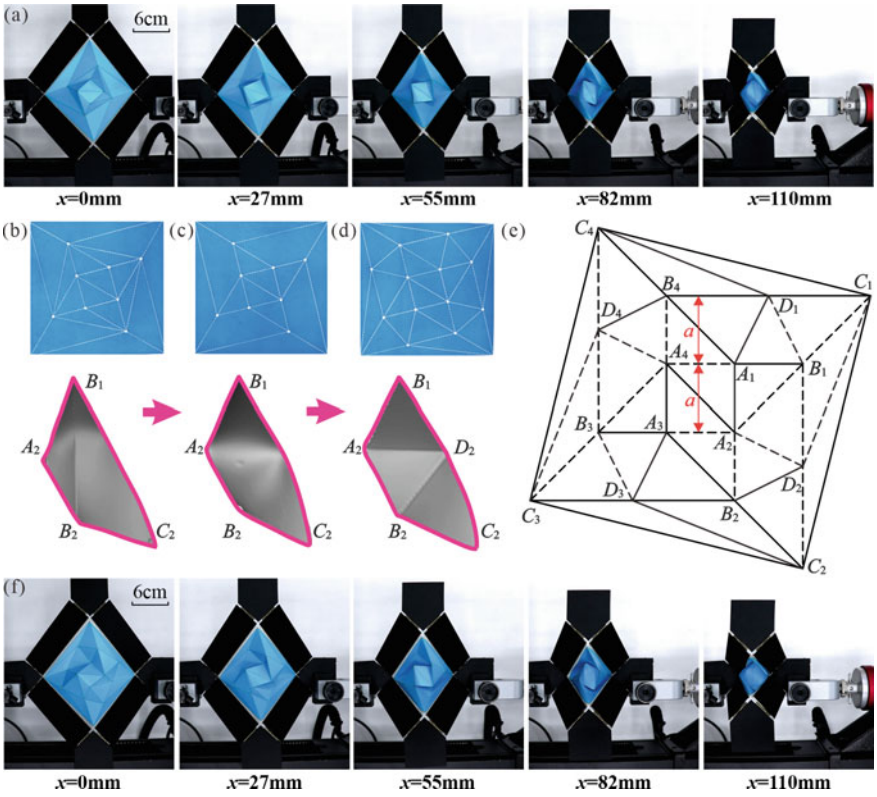

Fig. 3 Deformation mode and transformation of creases: **a** folding process of non-rigidly foldable winding origami pattern; **b–d** creases transformation patterns and their local deformation; **e** crease pattern of the new winding origami pattern; **f** folding process of the new winding origami pattern

and the outer boundary of the specimen is the same. Therefore, the boundary frame can play the dual role of boundary strengthening and loading. Fiber tape is used to bond the frame with the specimens.

To eliminate the prestressing effect of manual folding, heat treatment is carried out first. The initial distance of l_{C1C3} is fixed as $l_0 = 153.07$ mm. Then the fixed specimens are heated at 55 °C for 1 h in a constant temperature furnace. INSTRON 6800 testing machine is used for horizontal loading in the experiment with a loading speed of 50 mm/min. The experimental setup is shown in Fig. 2a. The initial position is l_0 for compression loading, and the displacement x is from 0 to 110 mm, corresponding to loading to the tight winding state point. In addition, 3D Scanner (Artec Space Spider, Artec 3D, Luxembourg) in Fig. 2b is also used to conduct a detailed analysis of the deformation modes of different patterns.

To eliminate the influence of the boundary frame's gravity and hinge stiffness, the test model is returned to the initial position after each experiment and reloaded

without the inner specimen in the same way. As the boundary frame has excellent repeatability, the data containing the specimen for the first time minus the data removing the specimen for the second time can be taken as the final result.

2.2 Deformation Mode and Crease Transformation

The folding process of the non-rigidly foldable winding structure is shown in Fig. 3a and the position of $x = 55$ mm in the figure corresponds to the self-locking point position. It can be seen that part of the creases is distorted due to the panel extrusion, while other parts of the crease still rotated as the simulation relation in the non-rigid stage.

It is found that the deformation of the panels in the non-rigid stage mainly concentrates on the four isosceles trapezoidal regions of $B_1A_2B_2C_2$, $B_2A_3B_3C_3$, $B_3A_4B_4C_4$ and $B_4A_1B_1C_1$. These key areas are scanned as shown in Fig. 3b. The B_1B_2 (B_2B_3, B_3B_4, B_4B_1) crease is flattened in the second stable state and the $B_1A_2B_2$ and $B_1B_2C_2$ panels are bent. The deformation of the panel and crease is the reason for the bistable property.

B_1B_2 and the other three creases are considered to be the direct cause of discordant deformation because they gradually fail and flattened. The pattern after removing this type of crease is also scanned at the same loading position in Fig. 3c. The isosceles trapezoid region will undergo bending deformation in the whole folding stage. Its deformation mode can be equivalent to the virtual crease of three triangles as panel bending. Two newly generated creases are a mountain line and a valley line, and their intersection point is a newly formed virtual node, as the midpoint of edge B_1C_2. Similarly, due to the generation of new nodes, the panel deformation of the outermost triangle $B_1C_1C_2$ also occurs, but the deformation degree is far less than that of the isosceles trapezoid region.

Real creases can greatly reduce panel deformation compared with virtual creases due to the weakening of materials. Therefore, the generated virtual creases are turned into real creases, and the new node is connected with the outermost intersection point as shown in Fig. 3d. It is important to note that there are other available ways to divide the outermost triangle $B_1C_1C_2$ and others, which hold the same effect. The new pattern as shown in Fig. 3e is also symmetric and the geometric dimension can be uniquely determined by the dimension variable *a*. 3D scanning result of the new pattern at the same loading position and in the same region is shown in Fig. 3d. As expected, the deformation of the panel in the trapezoidal region is significantly reduced. Therefore, the new pattern adapts to the geometric boundary of the trapezoid perfectly.

The deformation process of the new pattern is shown in Fig. 3f. The force–displacement curve and energy-displacement curve of the non-rigidly foldable pattern and the new pattern are shown in Fig. 4. Due to the thickness of the physical specimens, it will reach the tightly winding state point in advance, so the curve only shows the compression process of 100 mm. It can be seen from the results that the

non-rigidly foldable winding origami pattern self-locks in the position of displacement of about 55 mm, and then the reaction force rises rapidly, as the structure changes from the rigidly foldable stage to the non-rigidly foldable stage. The reaction force decreases rapidly after reaching the peak value near the displacement of 60 mm, and then transforms to the second stable point, showing the typical bistable characteristics. And the new pattern presents a gentle reaction curve. There is no obvious panel bending deformation under the whole loading. The reaction force of the new winding pattern is lower than that of the non-rigidly winding pattern. The reaction force of the new pattern decreases by 83.8% at the peak position of the non-rigidly foldable winding pattern. Similarly, it can be seen from the energy curve that the strain energy has a gentle trend in loading and a significant decrease compared with the non-rigidly foldable winding pattern. The total energy of the whole folding process decreases by 37.4%. The experimental results show that the panel deformation of the new pattern is less than that before transformation, but the kinematic proof to rigidly foldable is still needed.

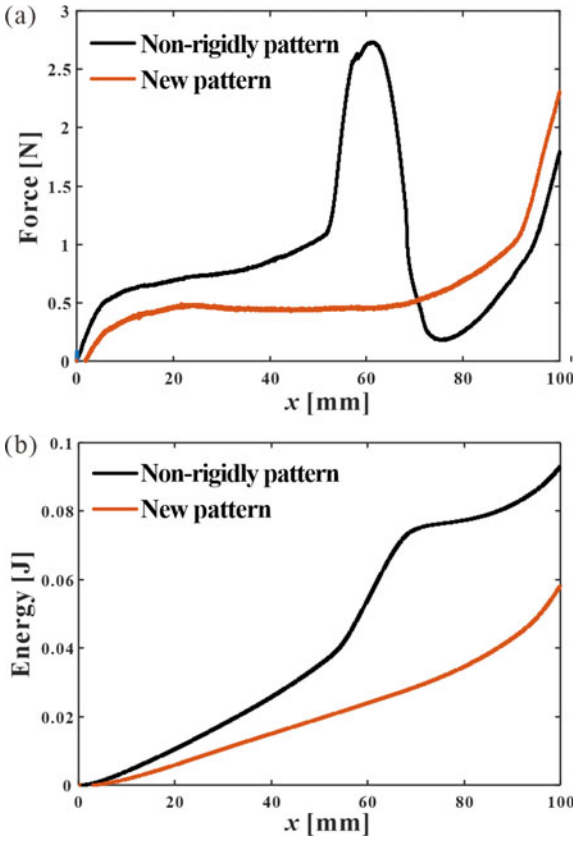

Fig. 4 Folding properties of the non-rigidly foldable winding origami pattern and the new pattern: **a** force–displacement curve, **b** energy-displacement curve

3 Kinematic Analysis of the New Pattern

The kinematic analysis of the new pattern is further carried out by the truss transformation method proposed by Yang et al. [24]. This method can simplify and eliminate the spatial over-constrained mechanism, and determine the degree of freedom of the spatial mechanism by using the Maxwell criterion and equilibrium matrix.

Specifically, the number of rods in the truss structure is denoted by b, and the number of spherical hinge points is denoted by j. The equilibrium matrix equation can be expressed as

$$\boldsymbol{At} = \boldsymbol{f} \tag{1}$$

where $\boldsymbol{A}$ represents the equilibrium matrix of $3j \times b$; $\boldsymbol{t}$ is a $b \times 1$ vector, representing the axial load per unit length of the rod; $\boldsymbol{f}$ is a $3j \times 1$ vector representing the load on the node. For the mechanism motion relationship, the truss structure could not bear the external load, then Eq. (1) can be converted

$$\boldsymbol{At} = 0 \tag{2}$$

According to Eq. (2), the number of self-stresses s and the number of mobility m can be obtained:

$$s = b - r \tag{3}$$

$$m = 3j - r - 6 \tag{4}$$

where r represents the rank of the equilibrium matrix $\boldsymbol{A}$.

As the origami panels in this work are all triangular, the creases and vertices can be directly replaced by rods and spherical hinges respectively. The truss form is shown in Fig. 5. The number of spherical hinge points $j = 16$, the number of rod members $b = 41$. The rank $r = 41$ of the matrix can be obtained through calculation. According to Eqs. (3) and (4), $s = 0$ and $m = 1$ can also be calculated, which proves that the new pattern is rigidly foldable with a single degree of freedom in the whole folding process.

The normal vector of the panel surface can be calculated through the coordinates of hinge nodes in different states. Then the variation relationship between the dihedral angles of all adjacent surfaces and the value of the input parameter (l_{C1C3}, which ranges from 174.9 to 42.43 mm) can be obtained.

To better analyze the function of creases, the creases of the new pattern are divided into transition creases and functional creases. The former ones are only to adapt to the geometric boundary generated by functional creases, whose dihedral angle increases from 0° and eventually return to 0°, including creases of A_2A_4, B_2D_2 (B_3D_3, B_4D_4, B_1D_1), A_2D_2 (A_3D_3, A_4D_4, A_1D_1) and D_2C_1 (D_3C_2, D_4C_3, D_1C_4). The functional creases play a major role in the winding function, whose angles increase from 0° to

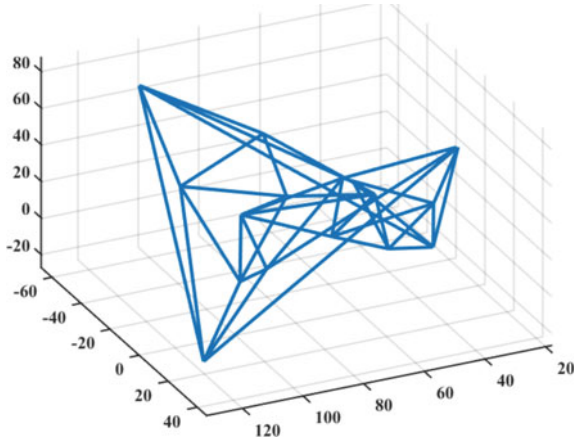

Fig. 5 Truss form of the new winding origami pattern

90° or 0° to 180°, including other creases except the transition creases mentioned above. Figure 6a is the dihedral angle relation curve of transition creases, and Fig. 6b and c are the dihedral angle of inner and outer functional creases respectively. The input l_{C1C3} is the distance between point A and point C. Due to the rotation symmetry of the structure, the dihedral angle characteristics of all types of creases are included in the figure.

The corresponding dihedral angle data obtained from the 3D scanning experiment are also included in Fig. 6, which are also obtained by calculating the normal vector of the spatial coordinates. The functional creases of the inner layer are completely blocked by the outer layer in the late folding stage, so only the data of the early stage can be measured. It shows that the experimental measurement results correspond well with the kinematic results of the mechanism on the whole, and the error of the outer transition crease C1D2 is relatively large due to its small angle change and proximity to the boundary. The folding process of the new pattern is built based on kinematics analysis, as shown in Fig. 7. Unlike the non-rigidly foldable winding pattern, the new winding structure remains rigidly folding from the flatted state point in Fig. 7a to the tightly winding state point in Fig. 7c without physical interference. Figure 7b is the loading position corresponding to the self-locking point of the non-rigidly foldable winding pattern, but self-locking does not occur. The deformation mode here is exactly the same as the experimental results in Fig. 3f which shows that the kinematic folding can be triggered without interference in the experimental model and the kinematic method is reliable.

4 Conclusions

In this paper, a non-rigidly foldable winding origami pattern is transformed into a rigidly foldable one successfully through the crease transformation, including

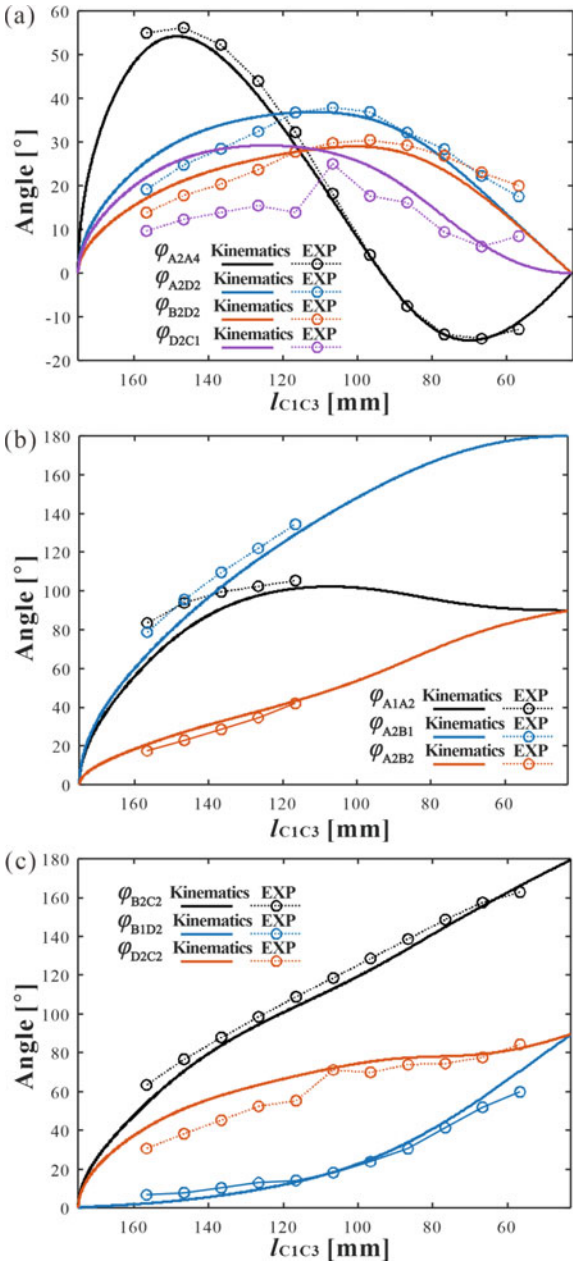

Fig. 6 Dihedral angle results of truss transformation and experiment: **a** transition creases, **b** inner functional creases, **c** outer functional creases

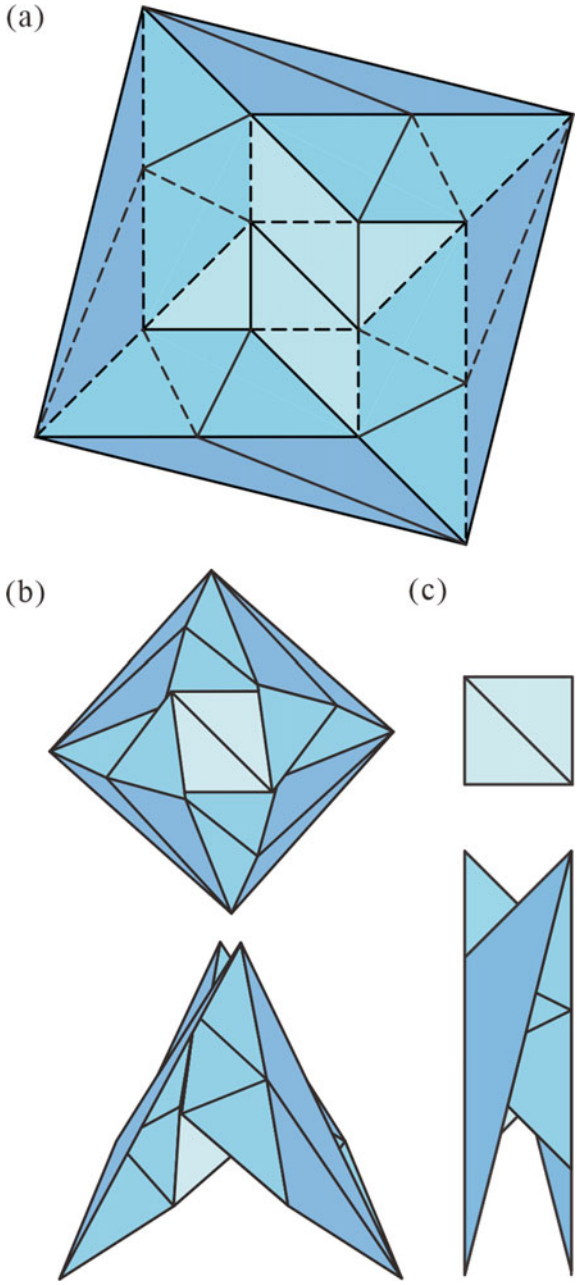

Fig. 7 The folding process of the new winding origami: **a** flat state point, **b** intermediate state point, **c** tightly winding state point

removing the creases in the region of concentrated deformation and then converting the newly virtual creases into the real creases. Firstly, the folding properties of the non-rigidly foldable winding origami pattern and the new pattern are tested, which shows that the new pattern greatly reduced the panel deformation and folding force. Furthermore, the truss transformation method is used to analyze the kinematics of the new pattern, and the rigidly foldable characteristic with a single degree of freedom is verified. Therefore, an innovative way to design new patterns based on experimental deformation is adopted in this work, that is, crease transformation is carried out in the deformation concentrated area, and the origami structure is successfully transformed from non-rigidly foldable mode to rigidly foldable mode. This provides a new idea for the design of rigidly foldable structure which is of significance. In addition, the newly-designed single-degree-of-freedom rigidly foldable winding origami structure has a great application prospect in space deployable structures and other fields.

Acknowledgements Supported by the National Natural Science Foundation of China (Projects 52035008, 51825503, 51721003) and the Tencent Foundation (XPLORER-2020-1035).

References

1. Miura, K., 1994, Map fold a la Miura style, its physical characteristics and application to the space science. Research of Pattern Formation, 77–90.
2. Miura K, Natori M (1985) 2-D array experiment on board a space flyer unit. Space Solar Power Review 5(4):345–356
3. Xiang X, Lu G, You Z (2020) Energy absorption of origami inspired structures and materials. Thin-Walled Structure 157:107130
4. Rus D, Tolley MT (2018) Design, fabrication and control of origami robots. Nat Rev Mater 3(6):101–112
5. Pesenti M, Masera G, Fiorito F (2018) Exploration of adaptive origami shading concepts through integrated dynamic simulations. J Archit Eng 24(4):04018022
6. Wang K, Chen Y (2011) Folding a patterned cylinder by rigid origami. Origami 5:265–276
7. Dai J, Jones JR (1999) Mobility in metamorphic mechanisms of foldable/erectable kinds. J Mech Des 121(3):375–382
8. Demaine ED, O'Rourke J (2007) Geometric folding algorithms. Cambridge University Press, Cambridge
9. Tachi T (2009) Generalization of rigid foldable quadrilateral mesh origami. Journal of the International Association for Shell and Spatial Structures 50(2):173–179
10. Watanabe N, Kawaguchi KI (2009) The method for judging rigid foldability. Origami 4:165–174
11. Peng R, Ma J, Chen Y (2018) The effect of mountain-valley folds on the rigid foldability of double corrugated pattern. Mech Mach Theory 128:461–474
12. Ma J, Chai S, Chen Y (2022) Geometric design, deformation mode, and energy absorption of patterned thin-walled structures. Mech Mater 168:104269
13. Silverberg JL, Na JH, Evans AA, Liu B, Hull TC, Santangelo CD, Lang RJ, Hayward RC, Cohen I (2015) Origami structures with a critical transition to bistability arising from hidden degrees of freedom. Nat Mater 14(4):389–393
14. Ma J, Song J, Chen Y (2018) An origami-inspired structure with graded stiffness. Int J Mech Sci 136:134–142

15. Xu, R., Zhang, X., Ma, J., Chen, Y., Cao, Y. and You, Z., 2018, "Folding a rigid flat surface around a square hub," ASME 2018 International Design Engineering Technical Conferences and Computers and Information in Engineering Conference, American Society of Mechanical Engineers, 51814, V05BT07A060.
16. Lee S, Shah SIH, Lee HL, Lim S (2019) Frequency-reconfigurable antenna inspired by origami flasher. IEEE Antennas Wirel Propag Lett 18(8):1691–1695
17. Guest, S. D., and Pellegrino, S., 1992, "In extensional wrapping of flat membranes," In Proceedings of the First International Seminar on Structural Morphology, Vol. 25.
18. Lang RJ (1997) Origami in Action. St. Martin's Griffin, New York
19. Kawasaki T (2005) Roses, Origami, & Math. Japan Publications Trading, Tokyo
20. Parque V, Suzaki W, Miura S, Torisaka A, Miyashita T, Natori M (2021) Packaging of thick membranes using a multi-spiral folding approach: Flat and curved surfaces. Adv Space Res 67(9):2589–2612
21. Liu, P., Ma, J., Chen, Y., Yuan, L., Zhao, H. and Wang, K., 2021, "The Kinematic Analysis and Bistable Characteristics of the Winding Origami Structure," International Design Engineering Technical Conferences and Computers and Information in Engineering Conference, Vol. 85451. American Society of Mechanical Engineers.
22. Zirbel SA, Lang RJ, Thomson MW, Sigel DA, Walkemeyer PE, Trease BP, Magleby SP, Howell LL (2013) Accommodating thickness in origami-based deployable arrays. J Mech Des 135(11):111005
23. Lang, R. J., Spencer P. M., and Larry L. H., 2016, "Single-degree-of- freedom rigidly foldable origami flashers," ASME.
24. Yang F, Chen Y, Kang R, Ma J (2016) Truss transformation method to obtain the non-overconstrained forms of 3D overconstrained linkages. Mech Mach Theory 102:149–166